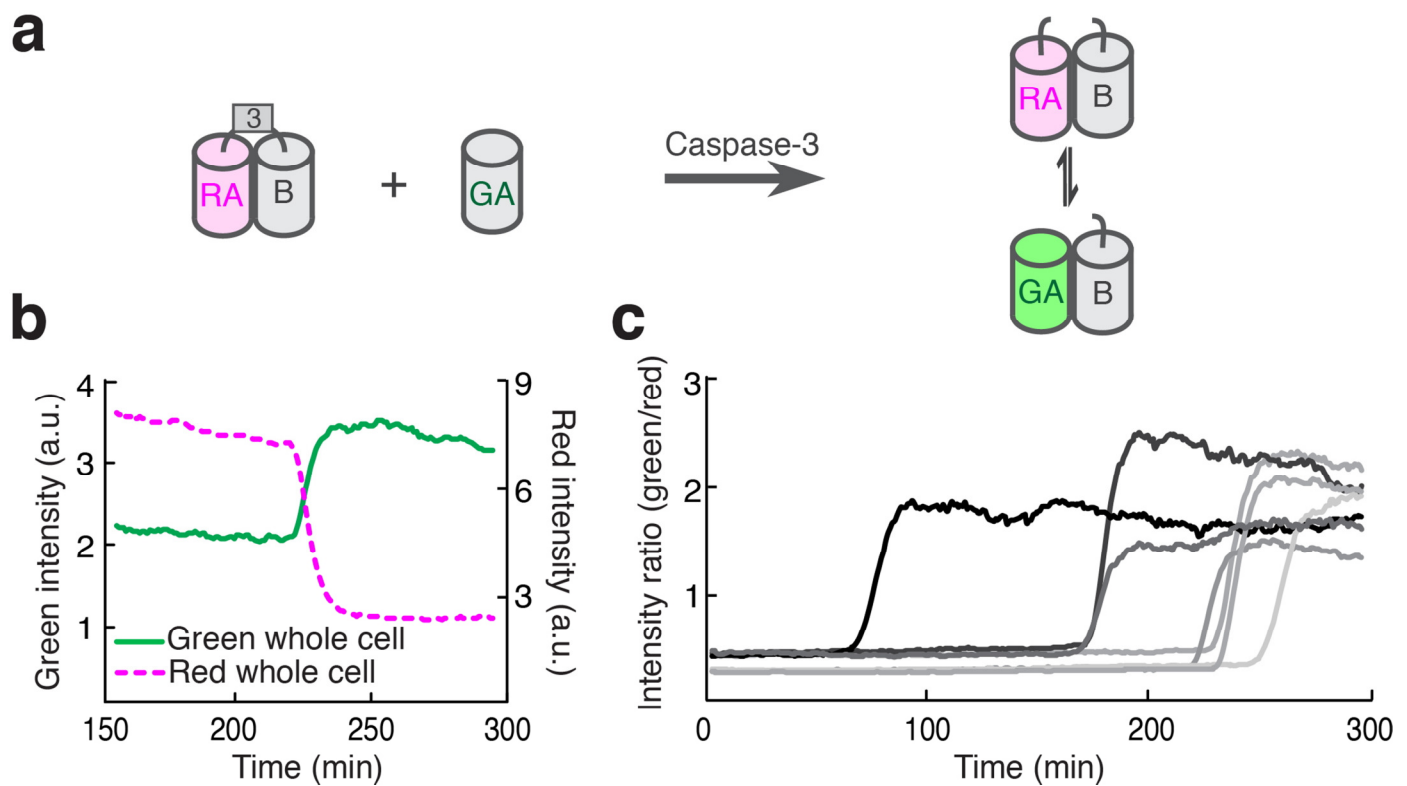


Supplementary Figure 1

B copies can rescue the fluorescence of the ‘wrong’ A copy partners.

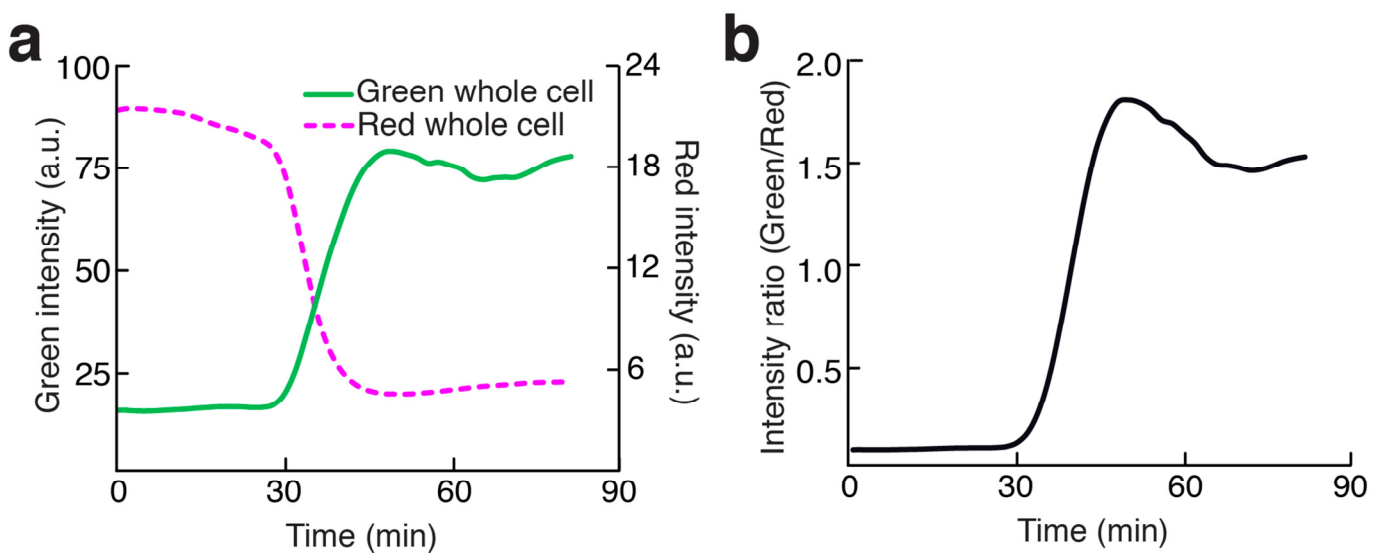
(a) The B copy (B1) originally engineered to rescue the fluorescence of GA is able to rescue the fluorescence of RA. (b) B1 with the K153E mutation (B2) is also able to rescue the fluorescence of both A copies. (c) The B copy (B3) originally engineered to rescue the fluorescence of RA complements both RA and GA with a K_d of $\sim 40 \mu\text{M}$. For the FPX strategy, a lower K_d will favor one interaction over the other, assuming equal concentrations of the two A copies (i.e., RA favored over GA for binding to B2). Due to its closely matched, and relatively low, affinities for both RA and GA, B3 is our preferred B partner. The identity of the B partner used in each biosensor construct is provided in **Supplementary Table 1**.



Supplementary Figure 2

Red-to-green FPX for detection of caspase-3 activity.

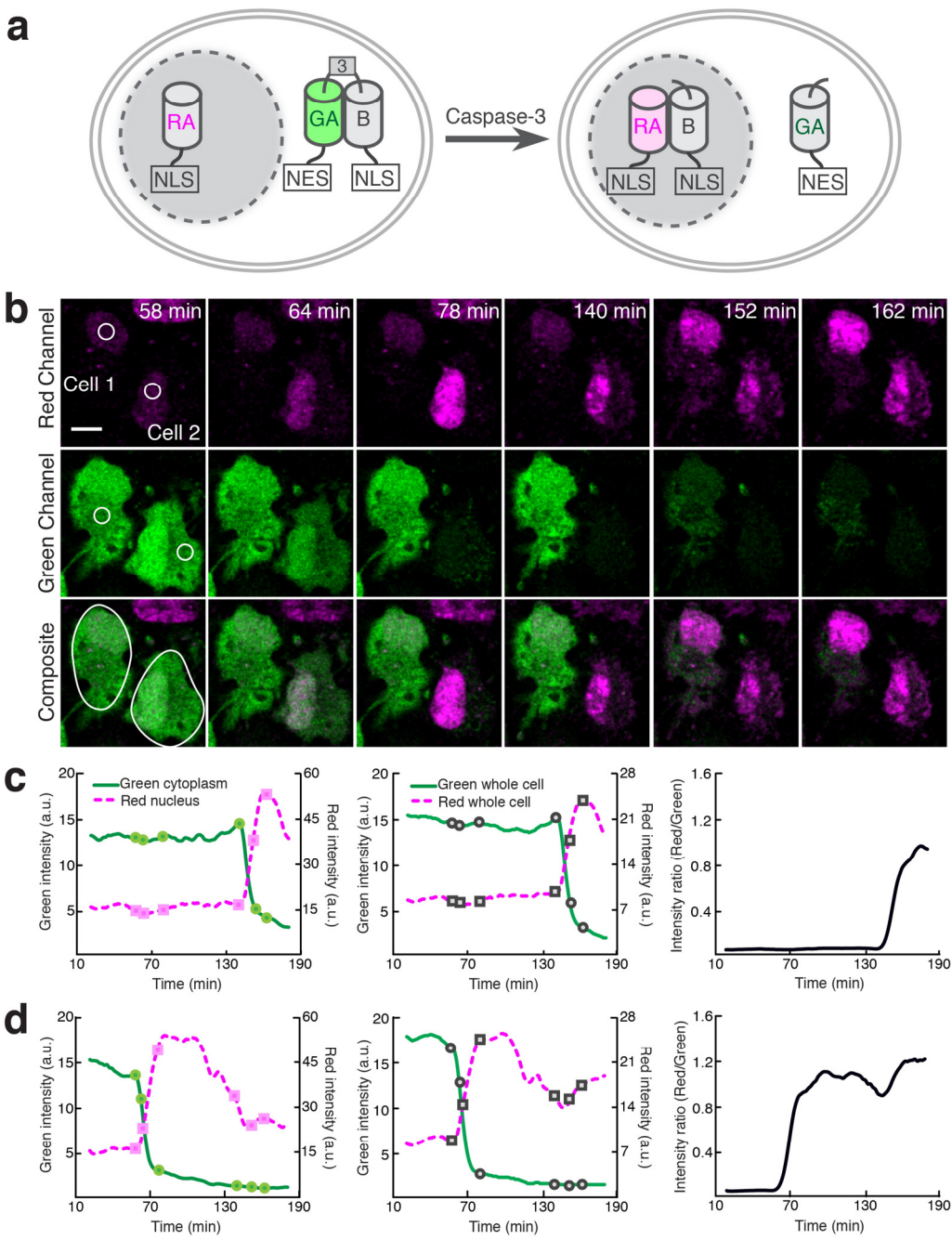
(a) Schematic representation of the biosensor. (b) Red and green whole cell intensities vs. time for a HeLa cell co-expressing RA-DEVD-B and GA and undergoing apoptosis. X-axis for all caspase activity imaging traces is time elapsed since 1 h after treatment with staurosporine. (c) Whole cell green-to-red intensity ratios vs. time for multiple cells treated and analyzed as in (b). Average green-to-red ratio change = 5.6 ± 1.6 -fold ($n = 7$).



Supplementary Figure 3

Representative whole-cell fluorescence intensity and ratio for the red-to-green protease biosensor based on translocation of the dark B copy, as shown in **Fig. 1e–g** and **Supplementary Video 2**.

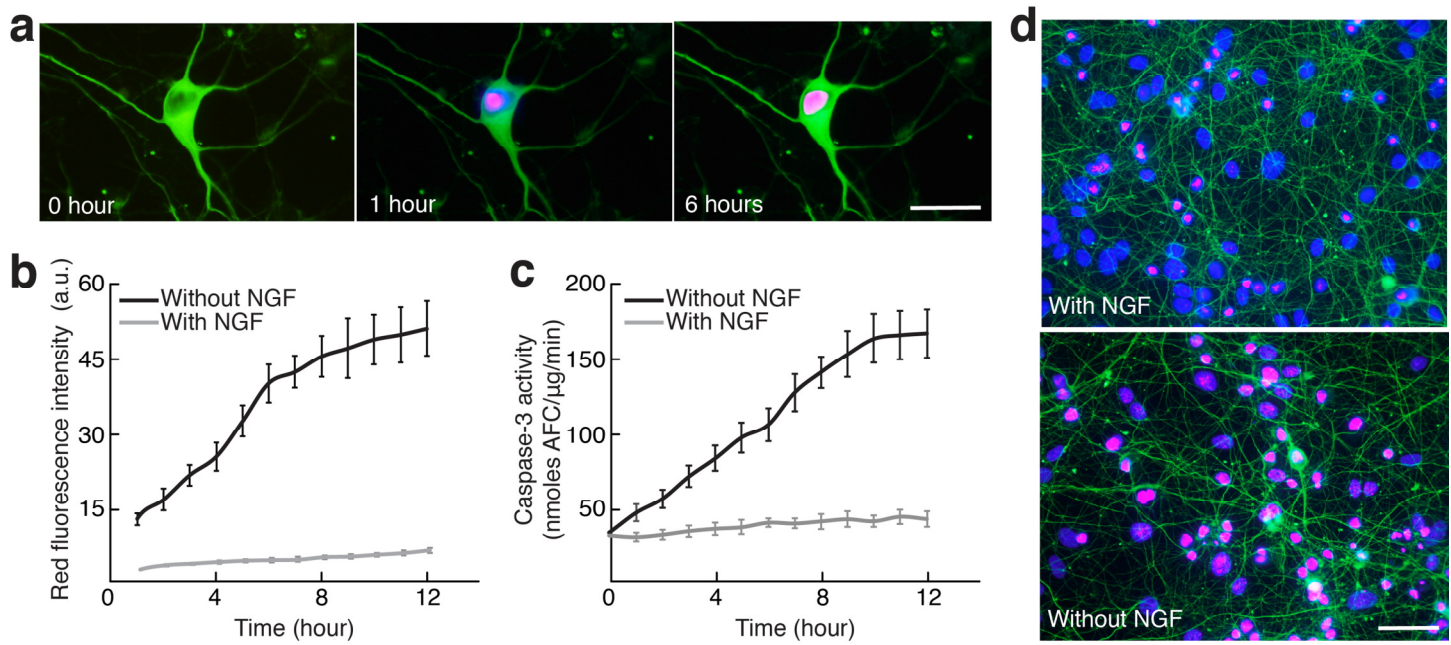
(a) Whole cell intensities in the green and red channels. The average red intensity decrease = 4.4 ± 1.6 -fold ($n = 6$) and the average green intensity increase = 4.7 ± 1.3 -fold ($n = 6$). **(b)** Whole cell green-to-red fluorescence ratio.



Supplementary Figure 4

Green-to-red FPX protease biosensor based on translocation of the B copy.

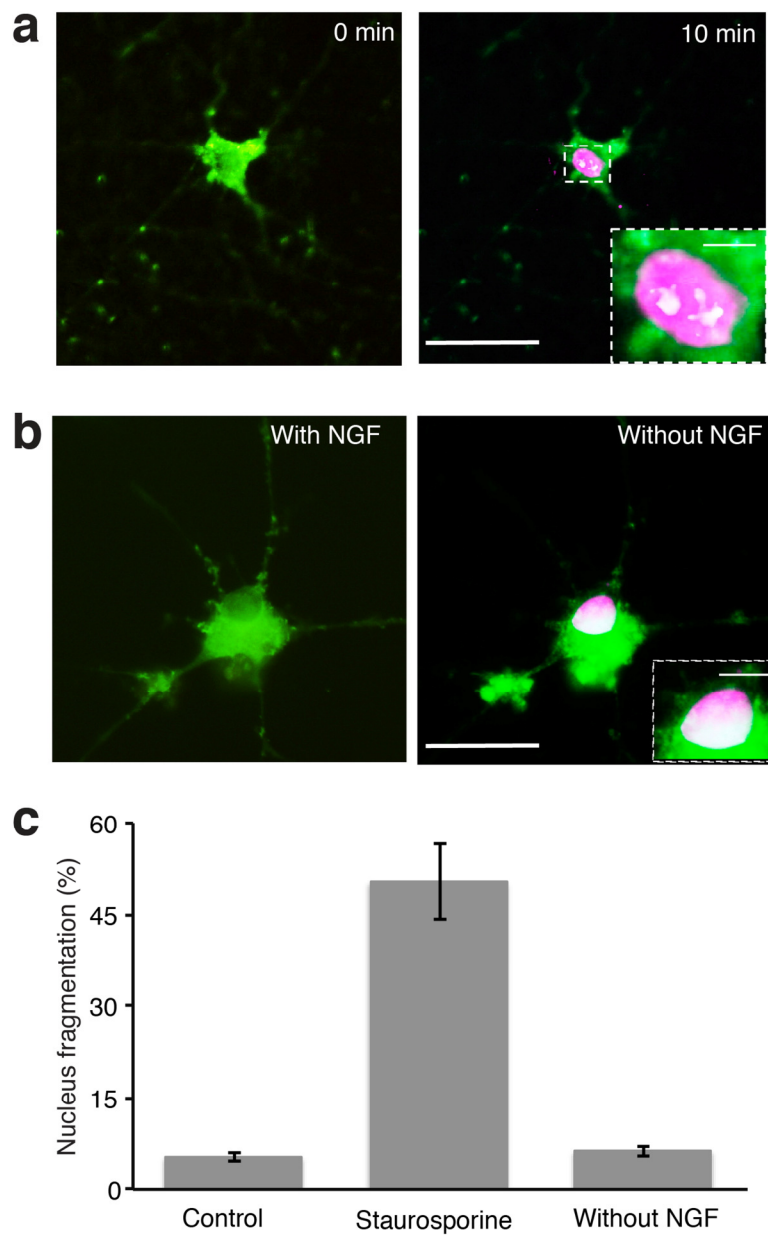
(a) Schematic representation of the biosensor. **(b)** Selected frames from imaging of HeLa cells co-expressing $\text{GA}^{\text{NES}}\text{-DEVD-B}^{\text{NLS}}$ and RA^{NLS} and undergoing apoptosis (**Supplementary Video 3**). Red fluorescence is represented as magenta. Scale bar represents 10 μm . **(c)** *Left panel:* Green cytoplasmic and red nuclear intensities vs. time for cell 1 using the ROIs represented in the left-most panels of the green and red channel images in **(b)**. Time points of cytoplasmic and nuclear ROIs corresponding to the frames in **(b)** are represented as circles and squares, respectively. *Middle panel:* Whole cell intensities vs. time for the cell 1 ROI indicated in the left-most composite image of **(b)**. Average green intensity decrease = 5.8 ± 1.7 -fold ($n = 3$) and average red intensity increase = 4.9 ± 0.8 -fold ($n = 3$). *Right panel:* Whole cell red-to-green ratio change using the data represented in the middle panel. **(d)** Data for cell 2, represented as in **(c)**.



Supplementary Figure 5

Imaging of caspase-3 activity during neuritic pruning.

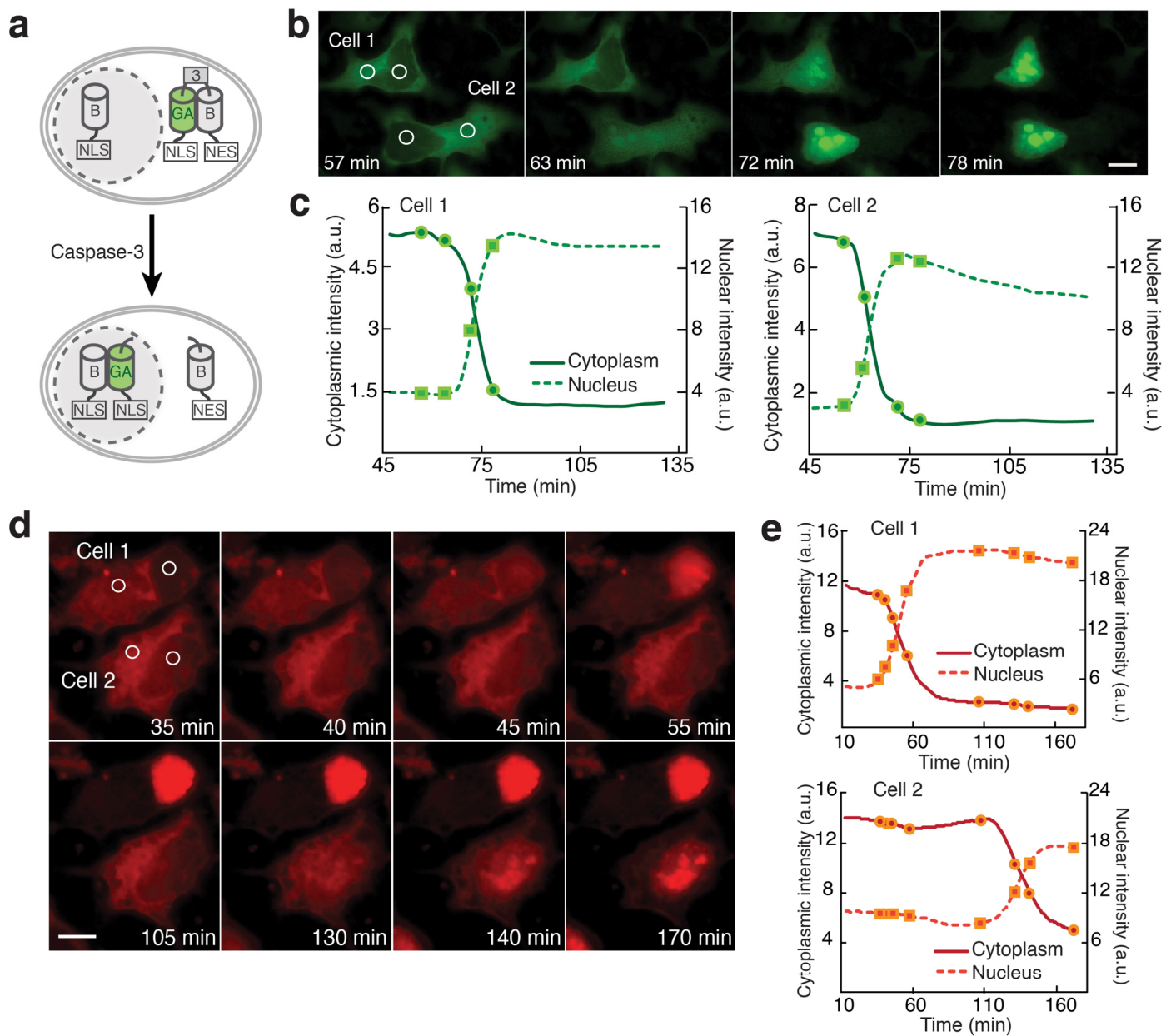
(a) Composite fluorescence images of a Hoechst (blue) stained neuron co-expressing GA^{NES} -DEVD-B $^{\text{NLS}}$ and RA $^{\text{NLS}}$ during nerve growth factor (NGF) deprivation. Scale bar represents 20 μm . (b) Nuclear red fluorescence intensity vs. time for neurons cultured with and without NGF ($p < 0.01$). During the first few hours of NGF depletion, the morphology of neurites remained unchanged, but the activation of caspase-3 could be monitored by the accumulation of red fluorescence in the nucleus. The diminished rate of increase from ~6 h (relative to in vitro measured caspase-3 activity as shown in (c)) is attributed to depletion of free RA $^{\text{NLS}}$. Error bars represent mean \pm SE. (c) In vitro measured caspase-3 activity vs. time for neurons cultured with and without NGF ($p < 0.01$). Error bars represent mean \pm SE. (d) Images of neurons cultured with or without NGF for 24 h. Following 24 h of NGF deprivation, neurons exhibited very little nuclear fragmentation, substantially fewer neurites relative to control, and brighter red fluorescence in the nucleus relative to control. Scale bar represents 50 μm .



Supplementary Figure 6

Neurons stimulated to undergo apoptosis exhibited increased nuclear red fluorescence and increased fragmentation compared to neurons deprived of nerve growth factor (NGF).

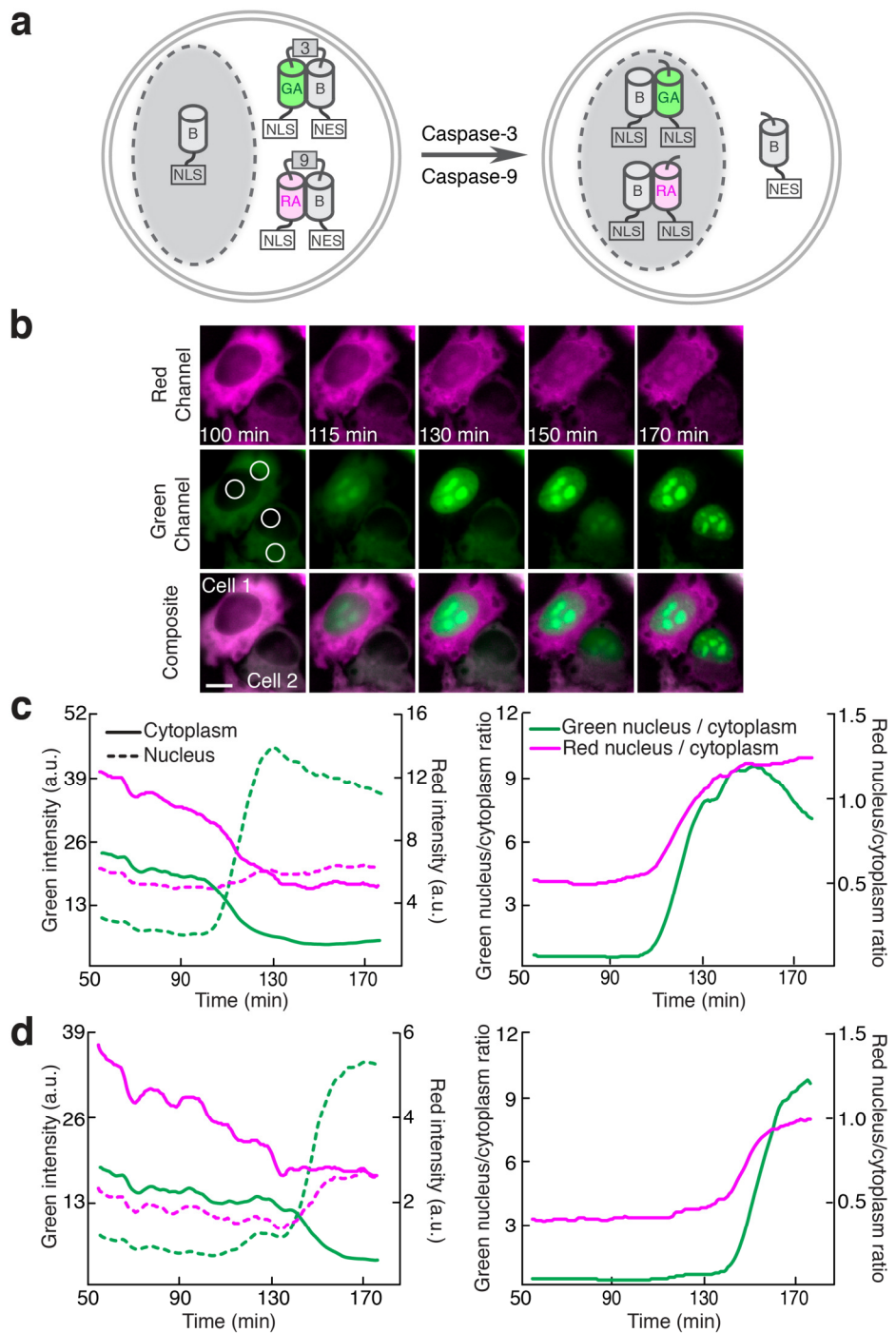
(a) Two color composite fluorescence images of a neuron during staurosporine-induced apoptosis. Scale bar represents 20 μm. *Inset:* Zoom-in showing nucleus fragmentation following caspase-3 activation during apoptosis. Scale bar represents 2 μm. (b) Images of a neuron before and after 24 h of NGF deprivation. Scale bar represents 10 μm. *Inset:* Zoom-in showing that the nucleus integrity was preserved. Scale bar represents 2 μm. (c) Quantification of nucleus fragmentation during apoptosis vs. NGF deprivation¹.



Supplementary Figure 7

Caspase activity sensing using FPX and translocation of the fluorogenic A partner.

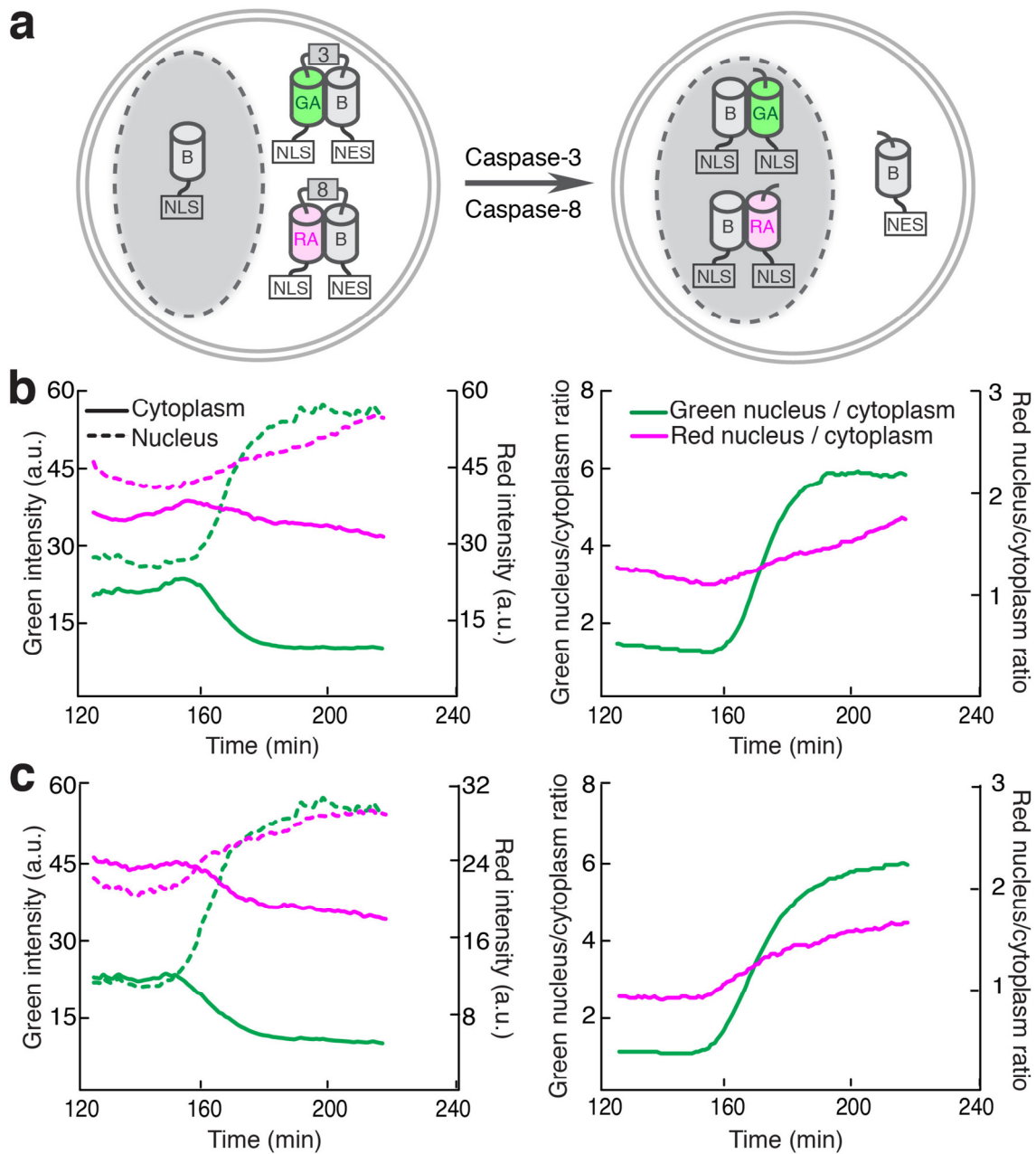
(a) Schematic illustration of the biosensor for caspase-3 activity with translocation of the fluorogenic GA partner. **(b)** Selected frames (see **Supplementary Video 4**) from imaging of HeLa cells co-expressing GA^{NLS}-DEVD-B^{NES} and B^{NLS} and undergoing apoptosis. Scale bar represents 10 μ m. **(c)** Intensity vs. time for the cytoplasmic and nuclear ROIs indicated in **(b)** with markers to indicate the time points for the images. The average maximum cytoplasmic intensity decrease = 2.5 ± 1.0 -fold ($n = 6$) and the average nucleus maximum intensity increase = 5.3 ± 1.2 -fold ($n = 6$). Subsequent apoptosis-associated fragmentation of the nucleus led to a decrease in the green fluorescence intensity in the nucleus. **(d)** Selected frames (see **Supplementary Video 5**) from imaging of HeLa cells co-expressing RA^{NLS}-DEVD-B^{NES} and B^{NLS} undergoing staurosporine-induced apoptosis. Scale bar represents 10 μ m. **(e)** Intensity vs. time for the cytoplasmic and nuclear ROIs indicated in **(d)**. Time points for the frames in **(d)** are represented as circles (cytoplasm) and squares (nucleus), respectively. The average cytoplasmic intensity decrease = 3.4 ± 1.3 -fold ($n = 5$) and the average nucleus intensity increase = 4.7 ± 2.9 -fold ($n = 5$).



Supplementary Figure 8

Two-color FPX with translocating GA (caspase-3) and RA (caspase-9) partners.

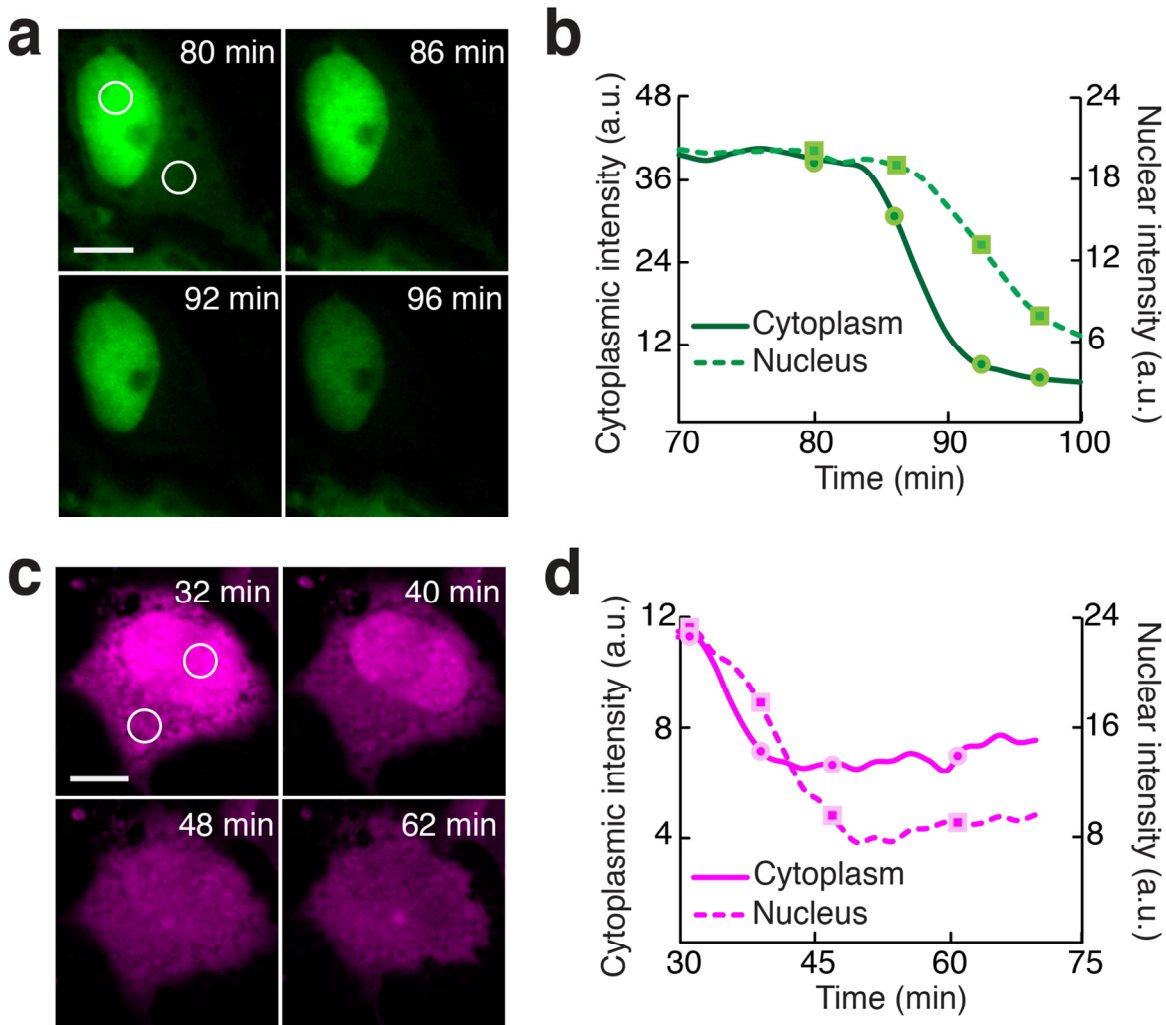
(a) Schematic illustration of strategy for monitoring both caspase-3 (green) and caspase-9 (red) activity with two different FPX constructs. (b) Selected frames from two-color imaging of tumor necrosis factor α (TNF α)-treated HeLa cells co-expressing RA^{NLS}-LEHD-B^{NES} (Ref. 2), GA^{NLS}-DEVD-B^{NES}, and B^{NLS}. Scale bar represents 10 μ m. See **Supplementary Video 6**. (c) Green and red fluorescence intensities in both ROIs (left hand panel) and green and red nucleus-to-cytoplasm intensity ratios (right hand panel) for cell 1 as labeled in (b). (d) Intensities and ratios for cell 2, represented as in (c). The average nucleus-to-cytoplasm ratio change for green and red fluorescence = 6.1 ± 1.5 -fold ($n = 3$) and 2.8 ± 1.1 -fold ($n = 4$), respectively.



Supplementary Figure 9

Two-color FPX with translocating GA (caspase-3) and RA (caspase-8) partners.

(a) Schematic illustration of attempted strategy for monitoring both caspase-3 (green) and caspase-8 (red) activity with two different FPX constructs. (b) Green and red fluorescence intensities for the nucleus and the cytoplasm (left hand panel), and green and red nucleus-to-cytoplasm intensity ratios (right hand panel), for a representative staurosporine-treated HeLa cells co-expressing RA^{NLS}-IETD-B^{NES} (Ref. 3), GA^{NLS}-DEVD-B^{NES}, and B^{NLS}. (c) Data for a second representative cell, presented as in (b). The average nucleus-to-cytoplasm ratio change for green and red fluorescence = 4.6 ± 1.8-fold ($n = 6$) and 1.5 ± 0.3-fold ($n = 6$), respectively. Consistent with a previous report⁴, we observe effectively simultaneous activation of both caspase-3 and caspase-8.

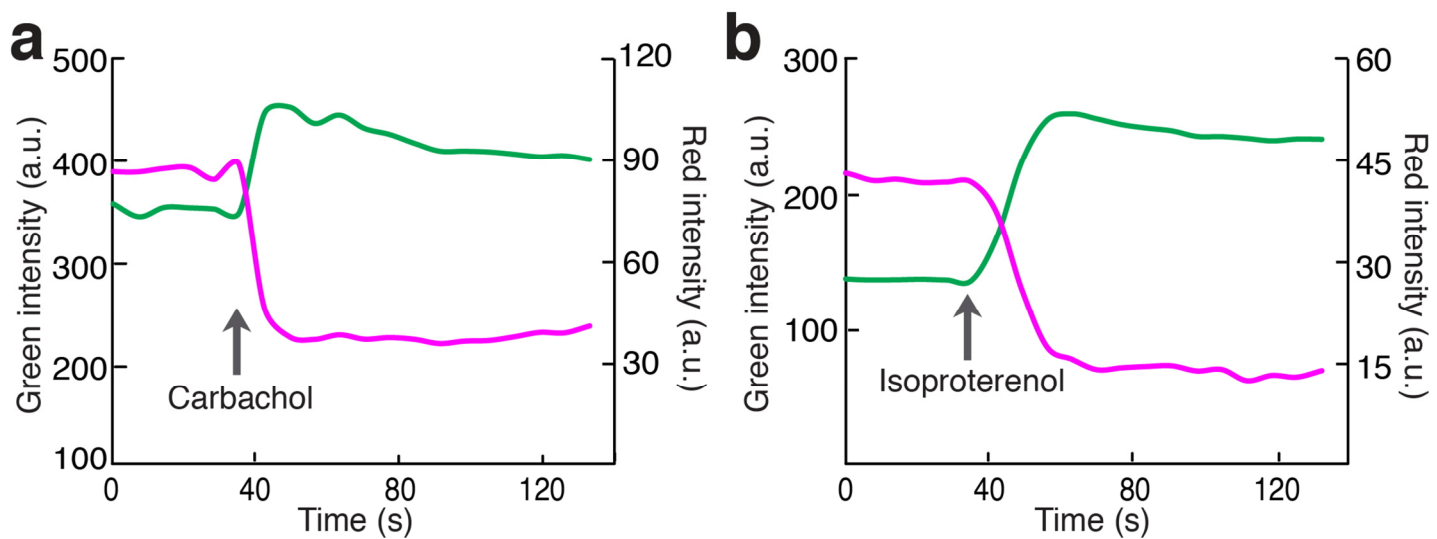


Supplementary Figure 10

Attempted caspase-dependent FPX with translocation from the nucleus to the cytoplasm.

(a) Selected frames from imaging of HeLa cells expressing GA^{NES} -DEVD-B^{NLS} and B^{NES} during staurosporine-induced apoptosis. **(b)** Intensity vs. time for the ROIs shown in **(a)**. **(c)** Selected frames from imaging of HeLa cells expressing RA^{NES} -DEVD-B^{NLS} and B^{NES} and undergoing apoptosis. **(d)** Intensity vs. time for ROIs shown in **(c)**.

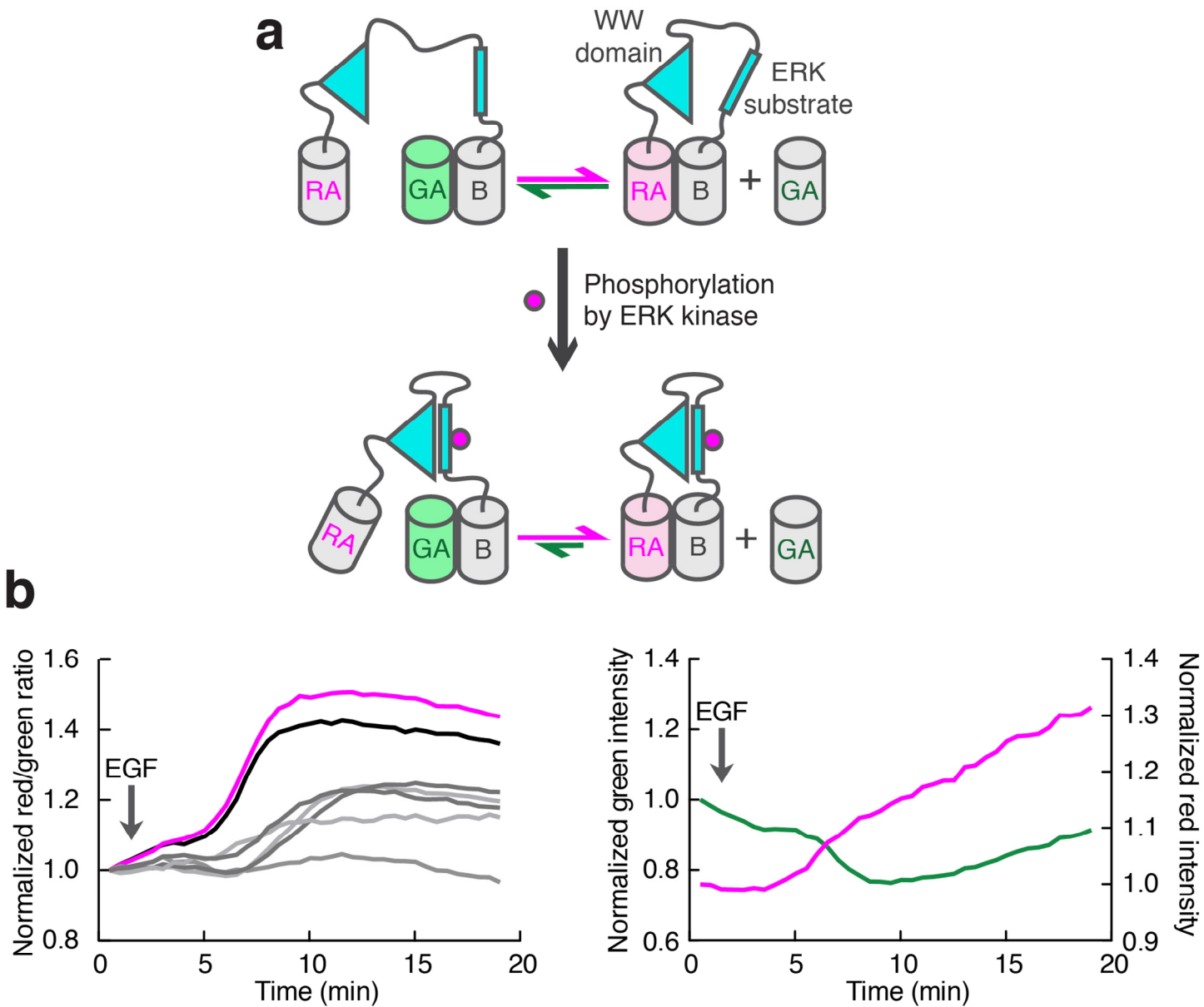
We suggest two possible explanations for these results. The first possibility is that A^{NES} (G or R) cannot be exported from the nucleus because the delayed activation of caspase-3 in the nucleus relative to the cytoplasm⁵ is causing a critical compromise in the integrity of the nuclear pore complex^{6,7}. The second possibility is that the larger volume of the cytoplasm relative to the nucleus is diluting the A copy to a concentration well below the K_d of the heterodimer (see **Supplementary Fig. 1**).



Supplementary Figure 11

Representative green and red intensity data for single cells expressing the PIP₂ biosensor or the cAMP biosensor.

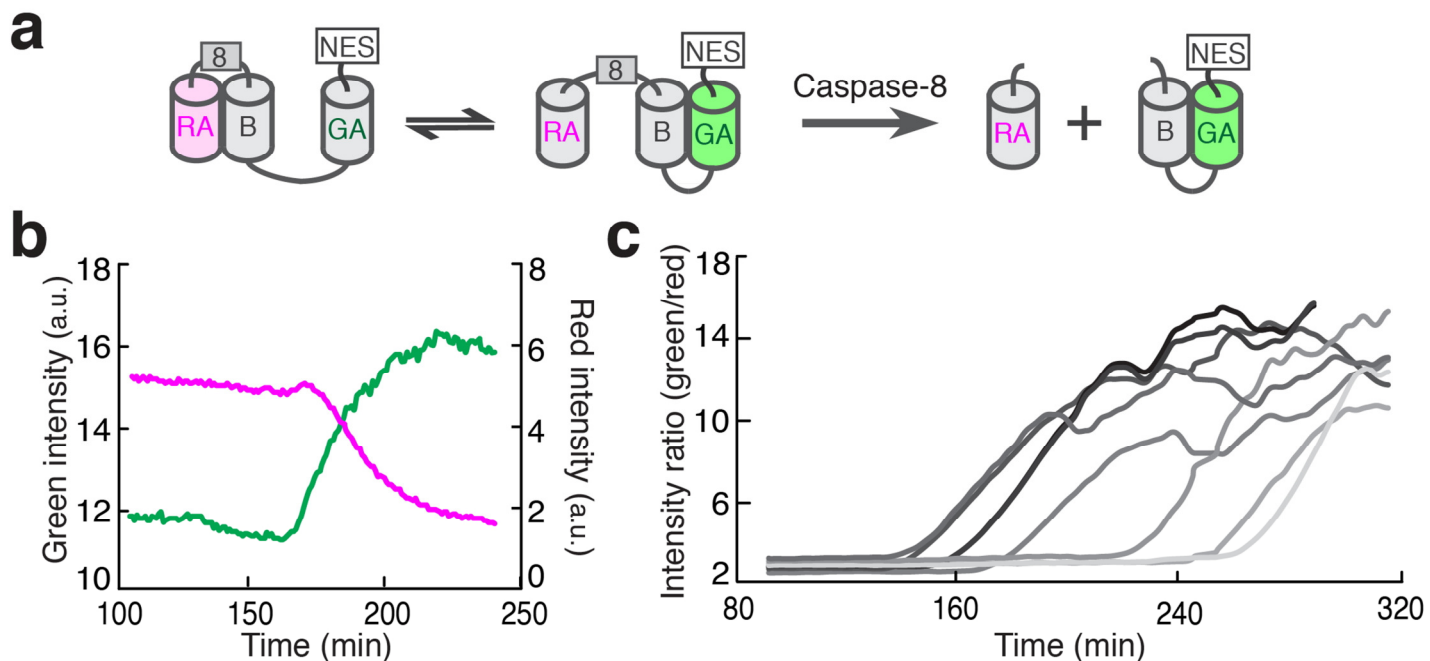
(a) Green and red intensity vs. time for a single cell expressing the PIP₂ biosensor represented in **Fig. 2d**. (b) Green and red intensity for a single cell expressing the cAMP biosensor represented in **Fig. 2f**.



Supplementary Figure 12

Ratiometric FPX for imaging of ERK activity using a single polypeptide RA–WW domain–ERK substrate–B protein and free GA^{NES}.

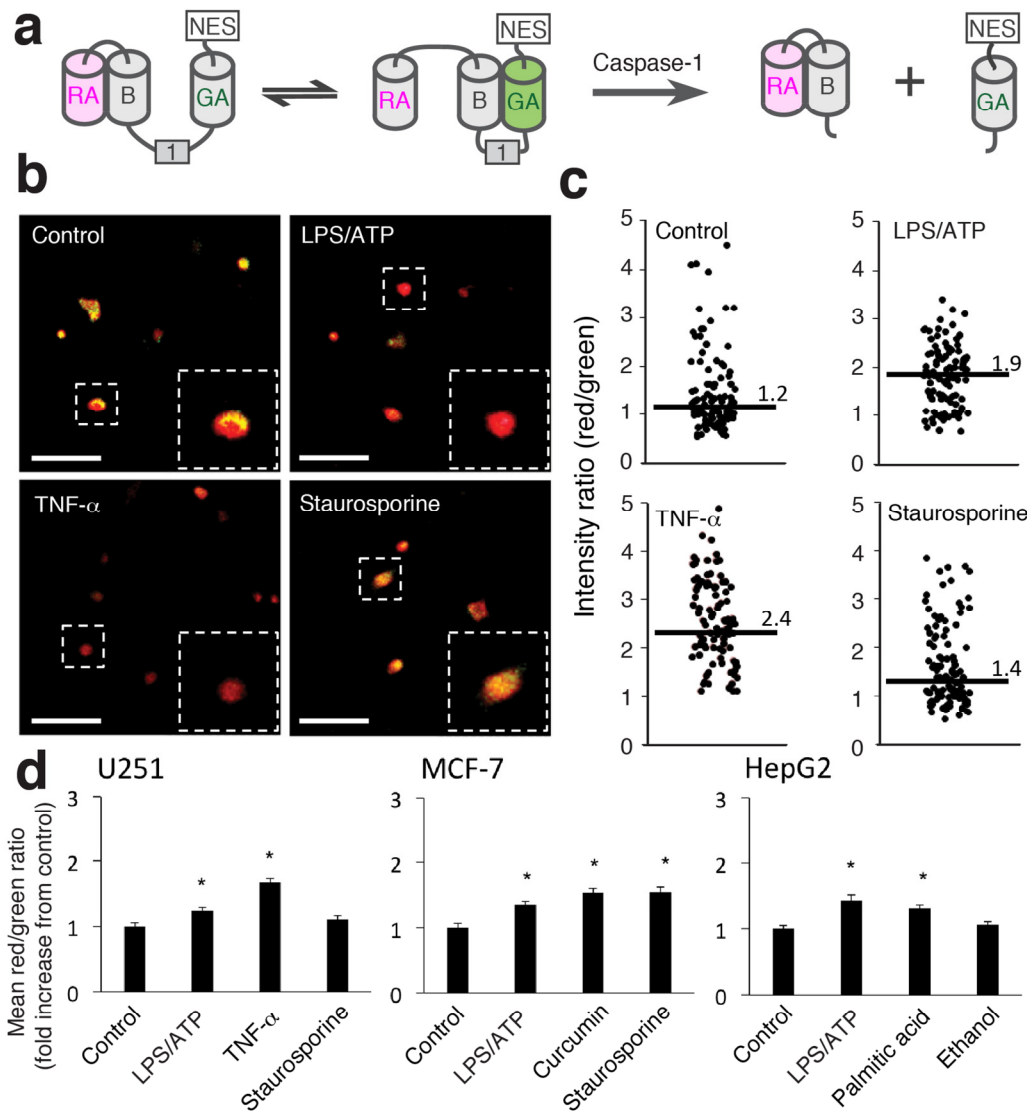
(a) Schematic of the ERK kinase activity reporter that rationalizes the observed ratio changes. In the absence of phosphorylation, either RA (intramolecular) or GA (intermolecular) can be bound to B. This equilibrium still exists in the phosphorylated form of the protein, but the association between RA and B is more favored due to the association of the WW domain and the phosphorylated substrate. **(b)** Ratiometric responses (left) and representative single channel intensity responses (right) of the cytosolic ERK kinase reporter co-expressed with GA^{NES} in HEK293 cells. Ratiometric intensity responses can clearly be seen approximately 5 min after stimulation with epidermal growth factor (huEGF, 100 ng/mL), consistent with results using a FRET-based biosensor⁸. The single channel intensity responses shown in the right panel correspond to the magenta trace on the left panel. Increases in the green and red channels after ~10 minutes are attributed to cell movement and morphological changes. These changes cancel out in the ratiometric plot, highlighting the advantage of ratiometric techniques such as FRET and FPX.



Supplementary Figure 13

Intramolecular FPX for imaging of caspase-8 activity.

(a) Schematic representation of a single polypeptide FPX biosensor for caspase-8. (b) Whole cell green and red intensities from imaging of HeLa cells expressing RA-IETD-B-linker-GA^{NES} and undergoing staurosporine-induced apoptosis. (c) Green-to-red intensity ratio vs. time for multiple cells treated and analyzed as in (b). The average green-to-red ratio change = 5.1 ± 0.8 -fold ($n = 8$). This intramolecular exchange approach is somewhat analogous to previously reported protease biosensors based on β -strand exchange within a single FP⁹.

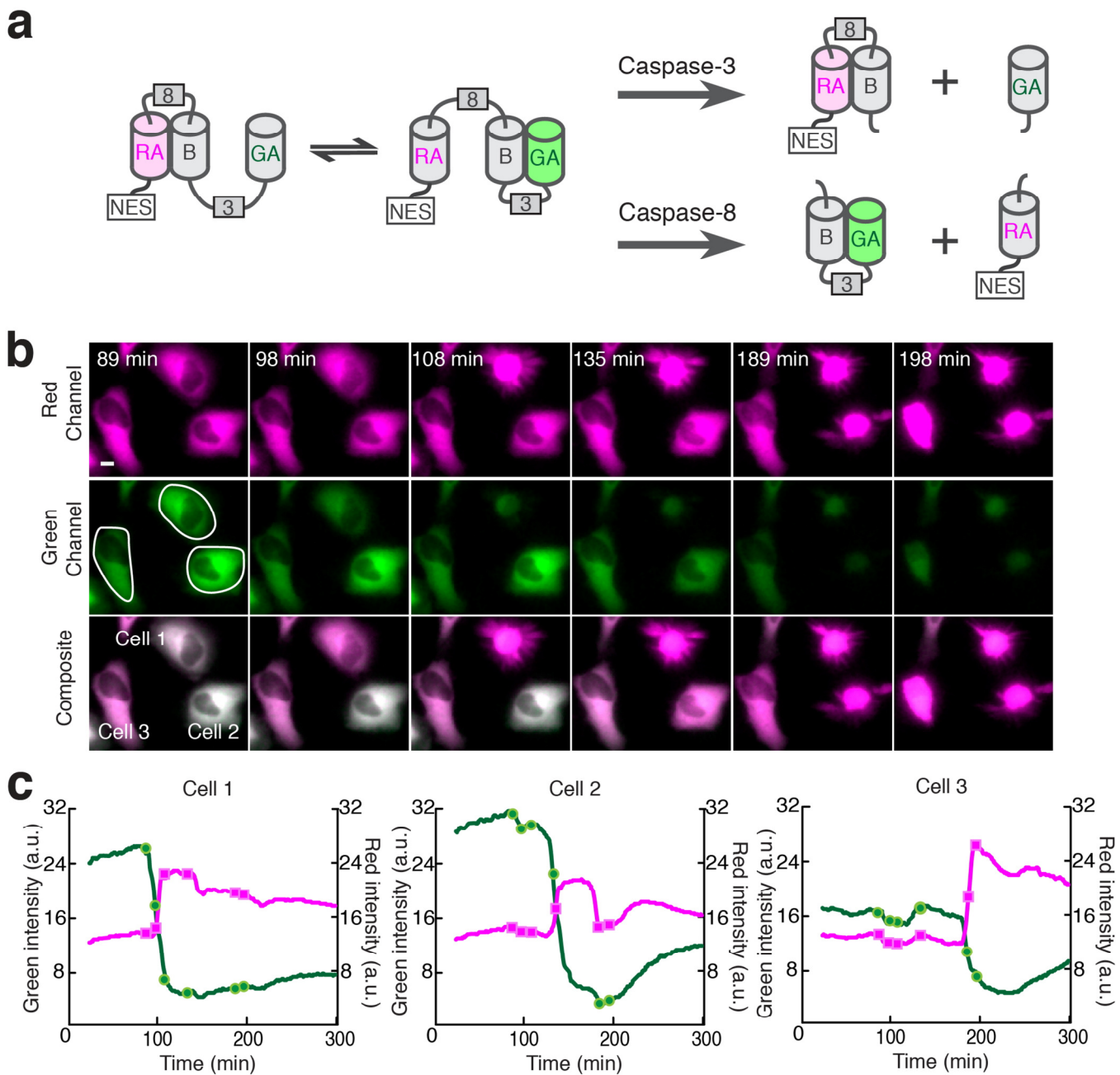


Supplementary Figure 14

Intramolecular FPX for imaging of caspase-1 activity.

(a) Schematic representation of a single polypeptide FPX biosensor for caspase-1. (b) Images of U251 glioblastoma cells expressing RA-linker-B-YVAD-GA and treated with inflammatory and non-inflammatory stimuli for 4 h. Scale bar represents 100 μ m. Inset: Zoom-in showing red and green fluorescence. (c) Whole cell red-to-green intensity ratios from imaging U251 cells ($n = 100$) treated as in (b). The black line indicates the median. (d) Whole cell red-to-green intensity ratios for U251, MCF-7 breast adenocarcinoma, and HepG2 liver carcinoma cells treated with inflammatory and non-inflammatory stimuli for 4 h. An increase in the red/green ratio indicates an increase in caspase-1 activity ($p < 0.01$). Mean values are expressed relative to the control set to 1. Error bars represent mean \pm SEM.

Adenosine triphosphate (ATP) in combination with lipopolysaccharide (LPS), a prototypical pyrogenic stimulus¹⁰, was found to promote caspase-1 activity in all three cell lines. MCF-7 cells, which lack caspase-3, displayed strong caspase-1 activation resulting from curcumin and staurosporine, two potent cytotoxic agents¹¹. In contrast, staurosporine did not stimulate caspase-1 activity in U251 cells, which instead undergo necrosis and caspase-3-mediated apoptosis¹². Glioblastoma cells strongly responded to the pro-inflammatory cytokine tumor necrosis factor alpha (TNF- α)¹³. In HepG2 cells, caspase-1 activity related to metabolic stress was induced using palmitic acid, a saturated fatty acid implicated in the metabolic syndrome¹⁴. Although pro-inflammatory pathways in hepatocytes are also up-regulated in chronic alcoholic hepatitis, acute stimulation of HepG2 cells with ethanol did not significantly induce caspase-1 activity at 4 h¹⁵.



Supplementary Figure 15

Intramolecular FPX for imaging of caspase-3 and caspase-8 activity using a single polypeptide.

(a) Schematic representation of the single polypeptide FPX biosensor for both caspase-3 and caspase-8. (b) Selected frames from imaging of HeLa cells expressing RA-IETD-B-DEVD-GA^{NES} and undergoing staurosporine-induced apoptosis. Scale bar represents 10 μ m. (c) Intensity vs. time of green and red fluorescence. Time points corresponding to the frames of green and red channel in (b) are represented as circles and squares, respectively. The average red-to-green ratio change = 7.9 ± 1.4 -fold ($n = 4$).

The mismatch in the amount of protease activity (i.e., caspase-3 cleavage (Fig. 3f) occurs more rapidly than caspase-8 (Supplementary Fig. 13c)) complicates the interpretation of these results and so we recommend the two-color translocation strategy shown in Supplementary Figs. 8 and 9 for imaging of two caspase activities.

Supplementary Table 1 | Details of the gene constructs used in this work.

Name	Gene	GenBank accession numbers	Addgene plasmid ID
GA ^{NLS} -DEVD-B ^{NES}	Xhol-GA-NLS-KpnI-DEVD-B3-NES-HindIII	KF976774	50835
RA ^{NLS} -DEVD-B ^{NES}	Xhol-RA-NLS-KpnI-DEVD-B3-NES-HindIII	KF976776	50840
RA ^{NLS} -IETD-B ^{NES}	Xhol-RA-NLS-KpnI-IETD-B3-NES-HindIII	KM979348	60972
RA ^{NLS} -LEHD-B ^{NES}	Xhol-RA-NLS-KpnI-LEHD-B3-NES-HindIII	KM979349	60973
B ^{NLS}	Xhol-B1-NLS-HindIII	KF976775	50836
GA ^{NES} -DEVD-B ^{NLS}	Xhol-GA-NES-KpnI-DEVD-B1-NLS-HindIII	KF976777	50842
RA ^{NLS}	Xhol-RA-NLS-HindIII	KF976778	50843
NES _{RA} -DEVD-B ^{NLS}	Xhol-NES-RA-KpnI-DEVD-B1 or B3-NLS-HindIII	KF976779	50849
GA ^{NLS}	Xhol-GA-NLS-HindIII	KF976780	50852
B ^{NES}	Xhol-B1 or B3-NES-HindIII	KP030819	61017
RA-DEVD-RB ^{NES}	HindIII-RA-KpnI-DEVD-B3-NES-Xhol	KP030818	36294
GA ^{NES}	Xhol-GA-NES-HindIII	KP030820	61018
GA-DEVD-GB ^{NES}	HindIII-GA-KpnI-DEVD-B1-NES-Xhol	KP030822	61020

RA ^{NES}	Xhol-RA-NES-HindIII	KP030821	61019
RA-CaM	HindIII-RA-KpnI-Calmodulin-NES-Xhol	KP030816	36292
M13-B	HindIII-M13-KpnI-B3-NES-Xhol	KP030817	36293
RA-IETD-B-DEVD-GA ^{NES}	HindIII-RA-KpnI-2×IETD-B2-BamHI-DEVD-GA-NES-Xhol	KM891584	60886
RA-linker-B-DEVD-GA ^{NES}	HindIII-RA-KpnI-Xhol-B2-BamHI-DEVD-GA-NES-Xhol	KM891581	60883
RA-IETD-B-linker-GA ^{NES}	HindIII-RA-KpnI-2×IETD-B2-BamHI-KpnI-GA-NES-Xhol	KM891582	60884
RA-CaM-B-M13-GA ^{NES}	Xhol-RA-KpnI-Calmodulin-BamHI-B3-EcoRI-M13-KpnI-GA-NES-HindIII	KM891585	60887
RA-linker-B-YVAD-GA	HindIII-RA-KpnI-Xhol-B2-BamHI-3×YVAD-GA-Xhol	KM891583	60885
PIP2_biosensor	NheI-RA-PH-2A-B3-PH-BssHII	KP001564	60936
cAMP biosensor	RA-PRKACA-2A-PRKAR2B-B3	KP001565	60937
ERK biosensor	BamHI-RA-BglII-WW_domain-KpnI-eevee_linker-ERK_substrate-Kpn1-B3-EcoRI	KM979350	60974

Supplementary Table 2 | List of oligonucleotides used in this work

Name	SEQUENCE (5' TO 3')
T7_seq_F (pcDNA_F)	TAATACGACTCACTATAAGGG
BGH_seq_R (pcDNA_R)	TAGAAGGCACAGTCGAGG
Xhol_ddFP_F	AATTCTCGAGAATGGTGAGCAAGAGCGAG
Xhol_ddGFP_B_F	ATGGCCTCGAGAGCCTCCGAGGACAACAAAC
ddFP_KpnI_R	ACCATGGTACCCCTGTACCGCTCGTCATGCC
KpnI_ddFP_F	CCGAGCGGTACCATGGTGAGCAAGAGCGAGGAG
ddGFP_A_HindIII_R	TTAATTAGCTTTAGGAGCTACCGCTGCCTGT
ddFP_HindIII_R	ATTAAGCTTTACTGTACCGCTCGTCATGCC
ddFP_NES_R	CTGGGGCATGGCACCGGCAGCACCTAGCCTGAAATTAGCAG GTCTTGATATCGGGAGCTAGCTCGAG
KpnI_DEVD_ddFP_F	AGAGAAAGGTAGGTACCGCCTCCGGCGATGAGGTGGATGGAG CCACCATCAAAGAGAGTTC
KpnI_IETD_ddFP_B_F	GCTCCGGTACCGCCTCCGGCATTGAGACCGATGGAGGCCACCAT CAAAGAGTTCATG
Quikchange_DEVD_to_IETD	GGTAGGTACCGCCTCCGGCATTGAGACGGATGGATCCACCATC AAAGAGTTCATGCG
Quikchange_DEVD_to_LEHD	GAAAGGTAGGTACCGCCTCCGGCTAGAGCATGATGGATCCAC CATCAAAGAGTTCATGCGCT
ddGFP_A_NES_R	CTCGAGCTAGCTCCGATATCAAGACCTGCTAATTCAAGGCTA AGGTGCTGCCGGTGCCATGCCAG
ddFP_NES_R	GCTCCCGATATCAAGACCTGCTAATTCAAGGCTAACATTGTACC GCTCGTCCATGCC
NES_KpnI_R	TCGAGGGTACCGCTCCGATATCAAGACCTG
NES_stop_HindIII_R	TCGAGAAGCTTTAGCTCCGATATCAAGACCTG
ddFP_link_R	GCTTCCCGCCGTTCCCTGTACCGCTCGTCATGCC
ddRFP_A_link_R	GCTTCCCGCCGTTCCCTGTACAGCTCGTCATGCC
Link_NLS_KpnI_R	TCGAGGGTACCTACCTTCTCTTTGGATCTACCTTCTC TTCTTTGGATCTACCTTCTCTTTGGATCGCTCCG CCGTTCC
Link_NLS_stop_HindIII_R	TCGAGAAGCTTACCTTCTCTTTGGATCTACCTTCT CTTCTTTGGATCTACCTTCTCTTTGGATCGCTCC GCCGTTCC

Kpn_2xIETD_ddFP_F	GCTCCGGTACCGCCTCCGGCATTGAGACCGATGGAGGTATCGA AACTGATGGCGGAGCCACCATCAAAGAGTTCATG
BamHI_DEVD_ddFP_F	AGCGGCAGCTCCGGATCCGCCCTCCGGCGATGAGGTGGATGGA GCCGTCAAAAGAGTT
ddFP_BamHI-R	GGAGGCGGATCCGGAGCTGCCGCTGCCGGTGTGCCCTTGTA CCGCTCGTCCATGCC
Remove_DEVD_add_KpnI_Quikchange	GATCCGCCTCCGGCGGTGCGGTGGTGGTACCGTCATCAAAG AGTT
Remove_2xIETD_add_Xhol_Quikchange	TACCGCCTCCGGCCTCGAGAGCGCTGGAGGTAGCGCATCTGG TGGCGGAGCCA
BamHI-3xYVAD_ddFP_F	CTCCGGATCCGGCTATGTGGCGGATGGATGGGCTATGTGGC GGATGGATGGGTTATGTGGCGGATATGGTGAGCAAGAGCGA GGAG
CaM_GSG_BamHI_R	CCATGGATCCACCGCTTCCCTTGCTGTCATCATTGTACAAAC TC
GSG_BamHI_ddFP_F	GGAAGCGGTGGATCCATGGTGAGCAAGAGCGAGGA
ddFP_ST_EcoRI_R	GTGGCGAATTCCGTGCTCTGTACCGCTCGTCCATGC
ST_EcoRI_M13_F	AGCACCGAATTGCCACCATGAAGAGGCCG
EKAR_BgIII_F	CCCAGATCTGGCGGACGAGGAGAACGCTGCC
EKAR_KpnI_R	GGCGGTACCCGGAAATTGGAATGACAGCTTGCTTATC
M13_KpnI_F	CCCGGTACCATGAAGAGGCCGCTGGCAGAAAACAGGCCATGCT
ddFP_A_BamHI_F	CCCGGATCCCATTGGTGAGCAAGAGCGAGGA
ddFP_A_BgIIIIns_R	CCGAGATCTGCTGCCGGTGCCATGCCCATGCCCCAGGTG
ddFP_B_EcoRIs_R	CCCGAATTCTTACTTGACCGCTCGTCCAT
pip2_1	AGCTGGCTAGCGTTACCATGGTGAGCAAGAGCGAGGAG
pip2_2	TTGAGCTCGAGATCTCTGTACAGCTCGTCCATGCC
pip2_3	AGATCTCGAGCTCAAGCTTCAATTCTGCA
pip2_4	ACTTCCTCTGCCCTCCTGGATGTTGAGCTCCTTCAG
pip2_5	GAGGGCAGAGGAAGTCTTCAACATGC
pip2_6	ACAGTCGAGGGCGCGCTACTGGATGTTGAGCTCCTTCAG
pip2_7	AGGCCCGGGATTCTCCACGTC
pip2_8	GAGAATCCCAGGGCTGTGAGCAAGGGCGAGGAGACC
pip2_9	AGCTGGCTAGCGTTACCATGGTGAGCAAGGGCGAGGAG
pip2_10	TTGAGCTCGAGATCTCTGTACCGCTCGTCCATGCC

pka_1	AGCTGGCTAGCGTTACCATGGTGAGCAAGAGCGAGGAG
pka_2	GGTGGAGGC GG TGAGGCAACGCCGCCGCCAAG
pka_3	TCCACCGCCTCCACCCTGTACAGCTCGTCCATGCC
pka_4	ACAGTCGAGGGCGCGCTAAA ACTCAGTAAACTCCTGCCAC
pka_5	AGCTGGCTAGCGTTACCATGAGCATCGAGATCCC GGCG
pka_6	TCCACCGCCTCCACCTGCAGTGGTTCAACAATATCCAT
pka_7	GGTGGAGGC GG TGAGT GAGCAAGGGCGAGGAGACC
pka_8	ACAGTCGAGGGCGCGCTACTTGTACCGCTCGTCCATGCC
pka_9	GAGAATCCC GGG CCTAGCATCGAGATCCC GGCG
pka_10	ACTTCCTCTGCCCTCAA ACTCAGTAAACTCCTGCC

References for Supplementary Figures

1. Qin, X.Y., Lv, J.H., Cui, J., Fang, X. & Zhang, Y. *Neurosci. Bull.* **28**, 606-610 (2012).
2. Thornberry, N.A. *et al.* *J. Biol. Chem.* **272**, 17907-17911 (1997).
3. Luo, K.Q., Yu, V.C., Pu, Y. & Chang, D.C. *Biochem. Biophys. Res. Commun.* **304**, 217-222 (2003).
4. Kominami, K. *et al.* *PLoS ONE* **7**, e50218 (2012).
5. Ai, H., Hazelwood, K.L., Davidson, M.W. & Campbell, R.E. *Nat. Methods* **5**, 401-403 (2008).
6. Ferrando-May, E. *Cell Death Differ.* **12**, 1263-1276 (2005).
7. Kramer, A. *et al.* *Proc. Natl. Acad. Sci. U. S. A.* **105**, 11236-11241 (2008).
8. Harvey, C.D. *et al.* *Proc. Natl. Acad. Sci. U. S. A.* **105**, 19264-19269 (2008).
9. Do, K. & Boxer, S.G. *J. Am. Chem. Soc.* **135**, 10226-10229 (2013).
10. Idzko, M., Ferrari, D. & Eltzschig, H.K. *Nature* **509**, 310-317 (2014).
11. Liang, Y., Yan, C. & Schor, N.F. *Oncogene* **20**, 6570-6578 (2001).
12. Couldwell, W.T. *et al.* *FEBS Lett.* **345**, 43-46 (1994).
13. Nabors, L.B. *et al.* *Cancer Res.* **63**, 4181-4187 (2003).
14. Joshi-Barve, S. *et al.* *Hepatology* **46**, 823-830 (2007).
15. Mandrekar, P. & Szabo, G. *J. Hepatol.* **50**, 1258-1266 (2009).